Polymer Journal (2016) 48, 689–696
© 2016 The Society of Polymer Science, Japan (SPSJ) All rights reserved 0032-3896/16
www.nature.com/pj

FOCUS REVIEW

Design of stimuli-responsive materials consisting of the rigid cylindrical inorganic polymer 'imogolite'

Kazuhiro Shikinaka

In this focused review, various stimuli-responsive materials that are prepared from the rigid rod-like polyelectrolyte 'imogolite' and constructed in accordance with its structural characteristics are described. The combination of imogolite and dicarboxylic acids yields hydrogels that exhibit thixotropy in response to mechanical shocks and physical anisotropy via the orientation of the imogolite during flowing and subsequent standing. Robust hydrogels have also been obtained by *in situ* polymerization of vinyl monomers in aqueous imogolite dispersions that show reversible isotropic–anisotropic structural transitions in response to strain. Furthermore, an electrorheological effect of the aqueous imogolite dispersions at extremely low voltage has been discovered that should permit the design of imogolite-based architectures as electro-stimulus-responsive materials.
Polymer Journal (2016) **48,** 689–696; doi:10.1038/pj.2016.12; published online 10 February 2016

INTRODUCTION

Some parts of living organisms consist of various nanofiber and nanotube architectures. For example, in cell cytoskeletons, semiflexible, rod/tube-like proteins such as filamentous actin and microtubules form network/bundle-like architectures via non-covalent bonds (for example, hydrogen bonding and electrostatic interactions).[1] These architectures facilitate motility and other various functionalities of cells through their keen stimuli-responsive structural transitions. Such materials capable of responding to stimuli such as light[2] and temperature[3] have been designed for *in vitro* systems through various opportune molecular assemblies and structures that are the basis of both emerging fields of scientific interest and new applications.[4] Rigid rod-like molecules have also been built as stimuli-responsive materials (for example, thermotropic/lyotropic liquid crystals[5–8]). Recently, novel stimuli-responsive materials consisting of rigid cylindrical inorganic polymers as an imitation/evolution of the architectures in the cell cytoskeleton were designed. This focused review describes the work toward the creation of novel functional materials that are based on the supramolecular architectures of rigid cylindrical polymers.

To create functional materials biomimetically, imogolite (henceforth denoted as IG) was used; it is a rigid fibrous molecule that forms a single-walled aluminosilicate cylindrical inorganic polymer with the composition $(HO)_3Al_2O_3SiOH$.[9–14] The external and internal diameters of IG are approximately 2 and 1 nm, respectively, whereas the length of IG can range from several tens of nanometers to several micrometers. Because IG is a perfectly rigid polyelectrolyte with a high aspect ratio,[15] it has been used as a constituent of inorganic–organic nanocomposites.[16] The outer and inner surfaces of IG are covered with $Al(OH)_2$ (proton-capturing) and Si(OH) (proton-releasing) groups, respectively. Thus the charge density of IG surfaces varies with the pH and ionic strength of aqueous media. Consequently, the dispersibility of IG in water changes drastically with pH; IG disperses as thin bundles or even as monofilaments in acidic and relatively low ionic strength aqueous media (pH≈4), resulting in opaque-to-transparent solutions. Hereafter, some developments of stimuli-responsive IG materials in accordance with the structural characteristics of IG has been presented.

THIXOTROPIC GELATION OF IGs

First, the stimuli-responsive material consisting of IG that exhibited non-Newtonian fluid behavior such as shear thinning was designed. Shear thinning, as well as stimuli-responsive liquid/solid phase transitions, known as 'thixotropy', are often found in the muscle and protoplasm[17] and are also important in many industrial processes (for example, paints and ceramic sols).[18] It has been posited that the formation of colloidal particle assemblies, generally called hydroclusters, is responsible for the emergence of shear thinning.[19,20] In my research,[21] IG purified by the appropriate procedures has been sonicated in pure water to obtain slightly opaque solutions with concentrations of 6.4 wt% (that is, 0.16 mol l^{-1} of aluminol groups) nanotubes with an average length of 68.5 nm. Such aqueous solutions have been used as starting materials throughout the experiments. It is well known that many types of inorganic and organic acids, such as carboxylic acids,[22] interact strongly with the outer surface of IG nanotubes. Because of the protonation equilibrium of the aluminol groups on the IG outer surface that forms cationic sites, the addition of carboxylic acids to IG creates strong hydrogen bonds or electrostatic interactions, wherein the $-Al(OH)_2$ unit acts as one equivalent functionality. When aqueous solutions of IG and maleic acid (MA), one of the typical short-chain dicarboxylic acids, are combined and aged, the resulting mixture yields opaque gels (Figure 1a; denoted as

Graduate School of Engineering, Tokyo University of Agriculture and Technology, Tokyo, Japan
Correspondence: Dr K Shikinaka, Graduate School of Engineering, Tokyo University of Agriculture and Technology, 2-24-16, Koganei, Tokyo 184-8588, Japan.
E-mail: k-shiki@cc.tuat.ac.jp
Received 17 November 2015; revised 5 December 2015; accepted 8 December 2015; published online 10 February 2016

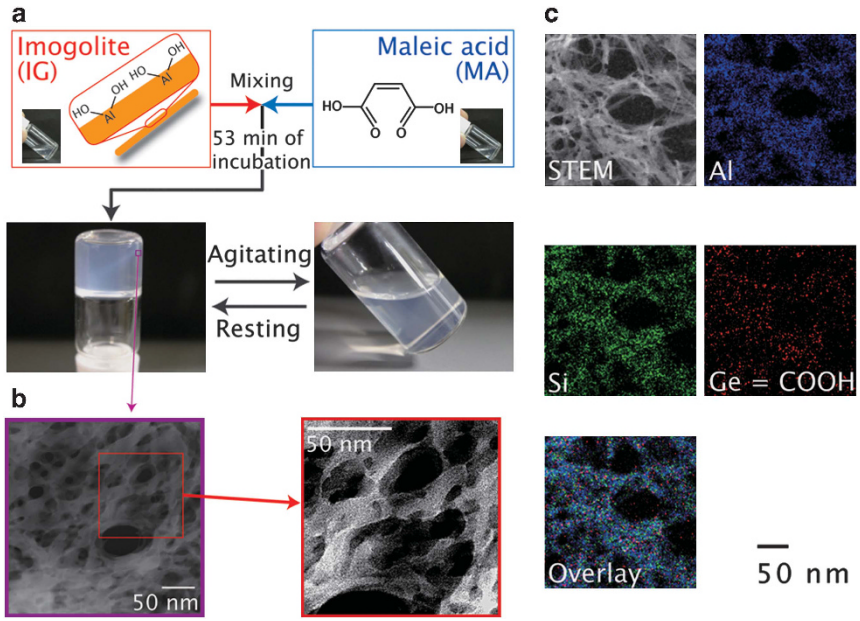

Figure 1 (**a**) Preparative procedure for an IG-MA gel and photographs of the sample tube inversion test for solid and liquid states. [-$Al(OH)_2$ of IG] = [MA] = 0.08 mol l^{-1}. (**b**) Cryo HAADF-STEM images of a rapidly frozen IG-MA gel. [-$Al(OH)_2$ of IG] = [DA] = 0.08 mol l^{-1}. (**c**) HAADF-STEM image and elemental mapping by energy dispersive X-ray spectroscopy of a dried mixture of IG, bis[2-carboxyethyl germanium(IV)] sesquioxide and MA. The Ge atoms (that is, carboxylic acids) localized on the IG nanotubes clearly indicate the presence of an interaction between dicarboxylic acids and IG nanotubes.

IG-MA gel) or hard-gel particle dispersions (phase-separated liquid/gel mixtures) with altered mixing ratios. If the ratio is not balanced, such that it is >2:1 or <1:4, the resulting mixtures exhibit apparent phase separation that produces hard-gel particles in aqueous medium.

When the mixing ratio, that is, the quantity of $-Al(OH)_2$ versus the molar ratio of MA (not the quantity of one $-COOH$ group), is near 1:1, the resulting sol-state mixture gradually turns into opaque gels with a thixotropic nature after approximately 1 h of aging at 25 °C (Figure 1a). In the rotating rheometric test, the aged IG-MA gel (sol) turns to the sol (gel) state within 6 s under agitation (rest) and vice versa accompanied by a perfect elastic modulus recovery.[22] The 1:1 combination of IG and dicarboxylic acids with 4–6 main-chain carbons similarly forms thixotropic gels but requires a longer ageing period to obtain the gel state. When IG is combined with oxalic or malonic acid at a ratio of 1:1, the mixture instantaneously forms turbid hard-gel particles dispersed in aqueous solution. Thus the gelation speed of the mixtures and their stimuli-responsiveness drastically changes with the number of main-chain carbons, configuration and steric hindrance of the dicarboxylic acids.

STRUCTURAL TRANSITION PROCESS OF IG GELS

Hereafter, the relationship between the microscopic structural changes and the thixotropic properties of the well-aged 1:1 IG-MA gel (sol) is described. To observe the microscopic structures of wet-state IG-MA gels, including the depth profile, wet-state gels (in the presence of water) were directly observed because the IG portions of the gel were composed of heavy atoms, which provided sufficient contrast. High-angle annular dark-field scanning transmission electron microscopy equipped with a cryo-sample transfer system (Cryo HAADF-STEM) was performed to observe *Z*-contrast images of silicone, aluminum and oxygen atoms. Figure 1b shows Cryo HAADF-STEM images of a torn sample of a quickly frozen IG-MA gel, corresponding to the images of the bulk and whole structures. The IG-MA gel consists of an interconnected, spongy framework. Because the STEM images and the energy dispersive X-ray spectroscopy atomic mapping coincide with each other, Shikinaka *et al.*[22] have determined that the IG nanotubes are the major component of the frameworks.

With contrast-intensified Cryo HAADF-STEM images (Figure 1b, right panel), the individual IG nanotubes in the frameworks of the IG-MA gels have been partly verified. As shown in this STEM image, the local structures of the IG-MA gel appear as crossed nanotubes. Furthermore, as shown in the HAADF-STEM images of the dried mixture of germanium-bonded dicarboxylic acids and IG (Figure 1c), the dicarboxylic acids attached to the IG surface indicate that dicarboxylic acids such as MA fully cover the IG surface in the mixture. Thus, in the present system, the MA-sheathed IG nanotubes behave as rod-like polyelectrolytes, and the outer $-COOH$ groups of the MA sheaths probably behave as linker groups for the cross-bridged nanotubes via inter-sheath hydrogen bonding. The frameworks constructed of cross-bridged, local structures in the IG-MA gels bring about the thixotropic properties of the gels.

Because of the presence of heavy atoms, the transient scattering profiles can be recorded by a time-lapse small-angle X-ray scattering (SAXS) technique that requires high contrast and resolution; periodic, rapid measurements at a 0.2-s interval were collected by using a tandem vertical undulator synchrotron radiation apparatus with high photon flux and an X-ray-counting, two-dimensional pixel detector. Supplementary Figure S1 illustrates the scattering profiles (the SAXS scattering curves, that is, the scattering intensity $\boldsymbol{I}(\boldsymbol{q})$ versus the scattering vector $\boldsymbol{q}$) of the well-aged IG-MA gel recorded at 0.2-s intervals during the cycles between the rest period (2 s) and the following vortex-mixing agitation period (2 s). Here the state of a rod-like substance can be evaluated from the steepness of the slope in the relation[23,24] $\boldsymbol{I}(\boldsymbol{q}) \sim \boldsymbol{q}^{-\mathbf{E}}$. Because the region $\boldsymbol{q} = 0.08$–$0.3\ \mathrm{nm}^{-1}$ is equal to the real-space size of IG nanotubes (68.5-nm average length and ~2.0-nm average external diameter), $\mathbf{E} = 1$ and 2 in this region corresponds to the IG nanotubes dispersed separately without forming assemblies and those fully packed in a unit space, respectively.[24]

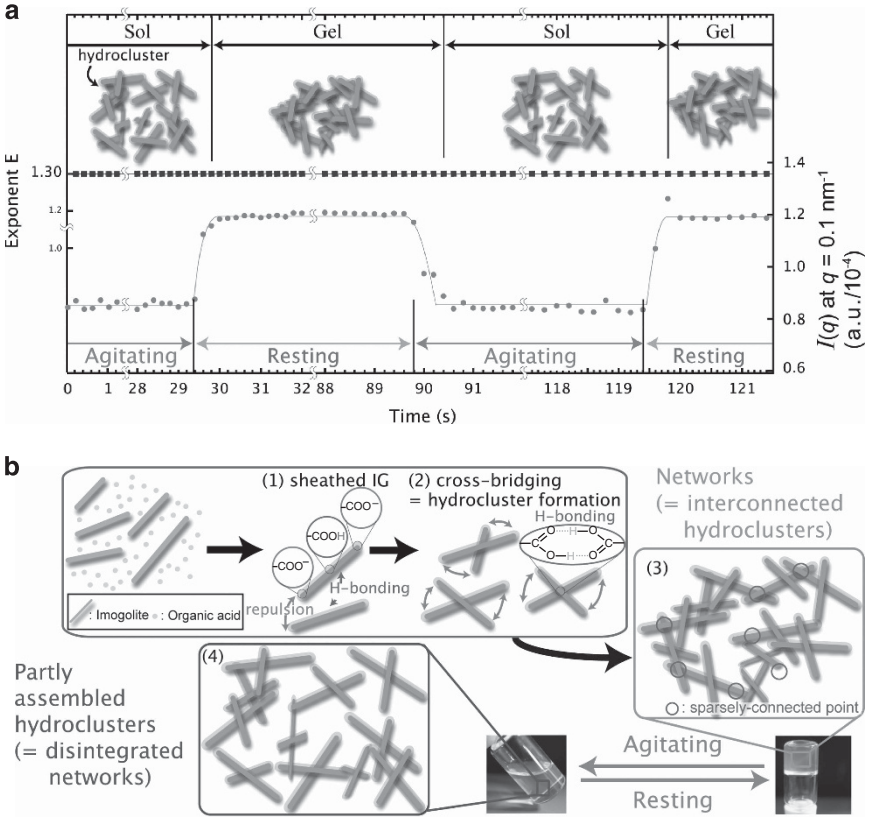

Figure 2 (**a**) Time dependence of $I(q)$ at $q = 0.1\ \mathrm{nm}^{-1}$ (closed circles) and **E** (closed squares) shown by time-lapse SAXS measurements of a well-aged IG-MA mixture ([-Al(OH)$_2$ of IG] = [MA] = 0.08 mol l^{-1}) in its gel/sol transition. These measurements were performed with 0.1-s X-ray irradiation at 0.1-s intervals. (**b**) Schematic illustration of the gelation and gel/sol transition of an IG-MA mixture, simplified using fewer rods than are in the actual system. The length of IG has a distribution.[14] This IG length distribution should bring about a density inhomogeneity of connected points (circles in (3)) between hydroclusters in the IG-MA gel, which causes a collapse of frameworks to partially assembled hydroclusters under agitation. Further details are described in the text. A full color version of this figure is available at the *Polymer Journal* online.

During the entire period of resting and agitating, the scattering function is characterized by the fixed asymptotic behavior of $I(q) \sim q^{-1.3}$ in the region of $q = 0.08$–$0.3\ \mathrm{nm}^{-1}$. Here **E** = 1.3 indicates the formation of some coarse structures,[23,24] which correspond to assembly units such as hydroclusters[12,13] in which the MA-sheathed IG nanotubes are sparsely packed. This indicates that the hydroclusters had previously existed, and the spatial packing density of the sheathed IGs in the hydroclusters is unchanged during all the rest/agitation processes. Meanwhile, $I(q)$ at $q = 0.1\ \mathrm{nm}^{-1}$ increases/decreases with the gelation/solation in response to resting/agitation, respectively, suggesting that the size of the networks composed of the interconnected hydroclusters fluctuates with the gelation and solation processes, as has been shown by other researchers.[25] As summarized in Figure 2a, $I(q)$, or the degree of the spatial extension of interconnected hydrocluster networks, is large in the gel state and small in the sol state, although the **E** value remains 1.3 during both gelation and solation. Because this $I(q)$ change is complete within 0.4 s of application or removal of agitation, the solation and gelation processes appears to be completed in a very short time, and the gel/sol or sol/gel transition occurs reversibly.

MECHANISM OF THIXOTROPIC GELATION IN IG-MA MIXTURES

According to the evidence, the structural change mechanism of the thixotropic IG-MA gel was proposed, as shown in Figure 2b. In the IG-MA system, the inevitable electrostatic repulsion suppresses the dissociation of the outer −COOH groups located in the middle positions of the sheathed nanotubes because of the high density of MA molecules in the sheath (Figure 2b (1)). Such non-dissociative outer −COOH groups may form inter-sheath hydrogen bonds, thus creating cross-bridged nanotubes, as well as intra-sheath (lateral) hydrogen-bonding networks. Meanwhile, the dissociation of outer −COOH groups of the MA sheath occurs at the edges of the nanotubes, as the electrostatic repulsion weakens at both edges. When the intra- or inter-sheath interactions and the dissociation of outer −COOH groups at the sheathed nanotube edges are balanced, it is possible to imagine the creation of 'cross-bridged nanotubes'. The cross-bridged nanotubes correspond to hydroclusters, as observed by Cryo HAADF-STEM and SAXS (Figure 2b (2)).[22,26] Such hydroclusters as basic units are further interconnected to form the frameworks of the gels (Figure 2b (3)). Because the electrostatic repulsion and the hydrogen bonding among hydroclusters coexist, the hydroclusters are weakly connected, resulting in inhomogeneous frameworks of gels that are easily collapsed from sparsely connected points (that is, the hydrogen bonds between the hydroclusters) under agitation (Figure 2b (4)) and re-structured upon resting (Figure 2b (3)). Thus the gels exhibit thixotropic properties; namely, the collapse of hydrogen bonds between the hydroclusters causes the shear thinning of the IG-MA gels, as shown in Figure 1a.

FLOW ORIENTATION OF IG IN THIXOTROPIC HYDROGELS

Because of the extremely fast thixotropic phase changes of the gel/sol or sol/gel transitions, which occur in < 1 s,[22] after flowing this

sol-state IG-MA gel through a cylindrical capillary cell (Figure 3a), the recovered gel state formed by an instantaneous stop in the flow exhibits an optical retardation and uniform birefringence along the flow direction (long axis of the cell) under a polarized optical microscope (POM). With respect to the flow direction, complete extinction at 0° and 90° was observed, and maximum brightness at 45° (Figure 3b), and color addition was also confirmed; these findings indicate that the IG nanofibers uniformly align in parallel with the flow direction, that is, the flow orientation of IG in the sol state is fixed by instantaneous gelation after the flow is stopped.

The uniform alignment of IGs collapses with mechanical impacts caused by the thixotropic nature of the oriented IG-MA gels; the introduction of interpenetrated networks (IPNs) is one plausible strategy to stabilize and fix their alignments. In Figure 3c, the shaping properties of the IPN gels prepared by the polymerization of 2-hydroxyethyl acrylate (HEA) and tetra(ethylene glycol) diacrylate (TEGDA) in IG-MA gel are compared. After polymerization in an X-shaped cell and equilibration in water, the IPN gel maintains the desired X shape, though the ordinary HEA gel is deformed under the same conditions by inevitable inhomogeneity appearing during network formation. The existence of IGs in the IPN gel reduces the inhomogeneity of the HEA network. Because the preparation of gels with desired shapes is made possible by the present IPN method, this strategy is expected to provide various types of soft materials that require fixed and complicated shapes, such as those used as artificial cartilage or blood vessel biomaterials.

The IG-MA gel mixed with HEA exhibits flow-orientation properties similar to those of the IG-MA gel (Figure 3b). Because the birefringence is unchanged before and after the polymerization of HEA and TEGDA, the resulting IPN gels maintain a uniform alignment provided by the flow orientation.[27] Polymerization after the flow orientation provides self-standing, oriented IPN gels (henceforth denoted as 'oriented IPN gels') with sizes as large as $42 \times 71 \times 2\ mm^3$ (Figure 4a).

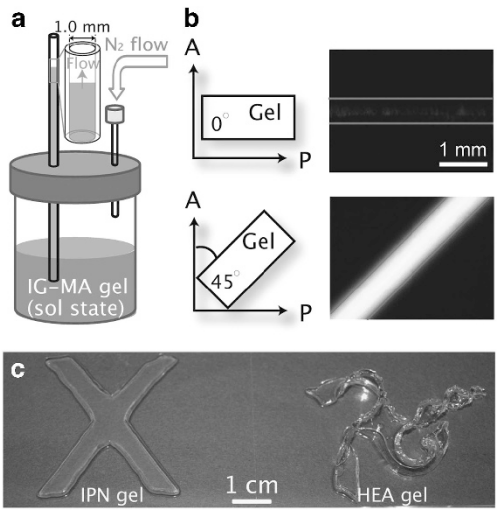

Figure 3 (**a**) Schematic illustration of the experimental setup for the flow-orientation capillary cell system. (**b**) POM images of the oriented IG-MA gel in the capillary cell, in which axes denoted by A and P represent the analyzer and polarizer setting direction, respectively. The angle between the gel and the analyzer is shown in the lower left of panel (**b**). The gray lines in panel (**b**) represent the capillary glass wall positions. (**c**) Photographs of an IPN gel (water content = 92.4%) and an HEA gel (as reference; water content = 96.8%) prepared by *in situ* polymerization in an X-shaped cell and subsequent equilibration in water for 7 days. A full color version of this figure is available at the *Polymer Journal* online.

The oriented IPN gels exhibit anisotropic mechanical properties, as shown in Figure 4b. Comparing parallel and perpendicular elongation with respect to IG orientation, the maximum fracture stress and initial tangent corresponding to Young's modulus are larger in the former by a factor of ~1.5 and 3, respectively. The oriented IPN gels also show anisotropic current–voltage characteristics.[27]

ROBUST IG HYDROGELS CONSISTING OF IG AND ORGANIC POLYMERS

As shown above, the combination of IG and an organic polymer network (that is, HEA gel) yields a self-standing hydrogel. On the basis of this result, hydrogels consisting of IG and various organic polymers, such as poly(acrylic acid) (PAA), poly(HEA) (PHEA), and poly (acrylamide) (PAAm) were synthesized to form robust hydrogels that depend on interaction between the IG and the organic polymers.

The phase states of the IG and organic polymer mixtures are shown in Figure 5a. The methods of mixing the IG and the polymers result in different mixture phase states. PAAm units and IG nanotubes appear to interact with each other through the $-NH_2$ or $>C=O$ and Si(OH) groups.[28] However, the combination of preformed PAAm ($4.0\ mol\,l^{-1}$) and IG (5.0 wt/v%) did not result in gel formation because PAAm does not interact with IG outer walls, and the penetration of macromolecular strands into the hollow structure of the IG nanotubes is rare. Based on these observations, the following two conclusions can be derived:

(1) Gels exhibit considerable mechanical strength because monomeric AAm molecules can penetrate the hollow tubes and then polymerize; and
(2) A few PAAm strands can be anchored to the ends of an IG nanotube to create pseudo-crosslinking.

Such pseudo-crosslinking could cause the IG-PAAm gel to display elastic properties when a large deformation is induced in the gels.

An addition of the preformed PHEA solution also results in a homogeneous mixture of [IG] (5.0 wt/v%) and [PHEA] ($1\ mol\,l^{-1}$). Use of a more concentrated PHEA solution results in the formation of local, hard gel-like precipitates, indicating sufficient interactions between IG and PHEA. Further investigation by using the *in situ* polymerization technique has revealed that the concentration of HEA units can be increased to $4.0\ mol\,l^{-1}$ to obtain macroscopically homogeneous gels.

Poly(carboxylic acid)s are known to interact with IG outer $Al(OH)_2$ groups by hydrogen bonding and related polar interactions.[22,29] However, such interactions are too strong and result in instantaneous phase separation and the formation of hard, solid particles upon the mixing of IG and preformed PAA in the concentrated state. However, mixing IG (5.0 wt/v%) with monomeric AA ($4.0\ mol\,l^{-1}$) results in a clear, homogeneous solution; the subsequent *in situ* polymerization produces clear, macroscopically homogeneous gels.

The stress–strain curves estimated from the tensile testing results on the IG-AAm, IG-HEA or IG-AA gels are illustrated in Figure 5b. The IG gels are tough, and their breakdown stress/strain and Young's modulus greatly depend on the type of vinyl monomers. The breakdown strain of the IG-AAm gel is larger than that of the other two gels, that is, the IG-AAm gel is more elastic than the other gels, owing to fewer pseudo-crosslinking IG-to-IG tying points than those formed by the outer sidewall anchoring in IG-HEA or IG-AA. This difference in tying is also reflected in the spatial density, or degree of

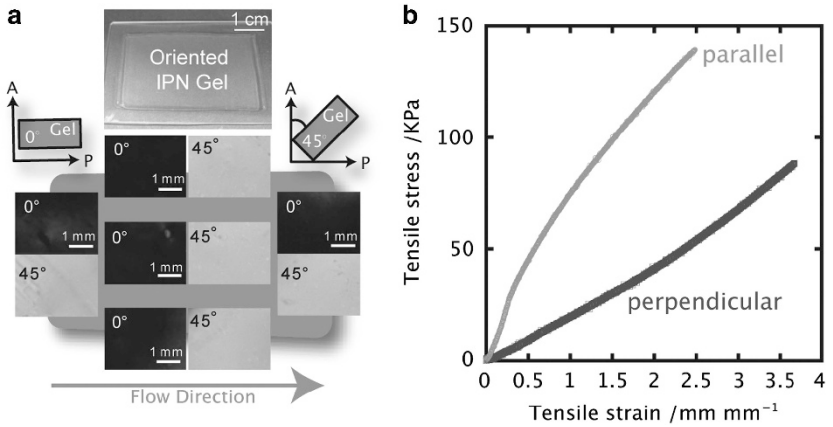

Figure 4 (**a**) Photographs (upper) and POM (lower) images of the oriented IPN gels prepared in a rectangular cell ($42 \times 71 \times 2$ mm^3). Background illustrations of the POM images correspond to the oriented IPN gels shown in the photographs. The birefringence value of the oriented IPN gels became as large as 1.64×10^{-4} at flow velocity = 34.9 ml min^{-1}. (**b**) Typical tensile stress–strain curves of wet-state oriented IPN gels measured from parallel and perpendicular stretching with respect to IG orientation. A full color version of this figure is available at the *Polymer Journal* online.

a

Polymer	Mixing method	Conc. (mol/L)	Phase of mixture
PAAm	Preformed polymer	4.0	No gels
	In situ polymerized	4.0	Gelation
		2.0	Gelation
PHEA	Preformed polymer	1.0	No gels
	In situ polymerized	4.0	Gelation
PAA	Preformed polymer	1.0	Precipitation
	In situ polymerized	2.0	Gelation
		4.0	Gelation

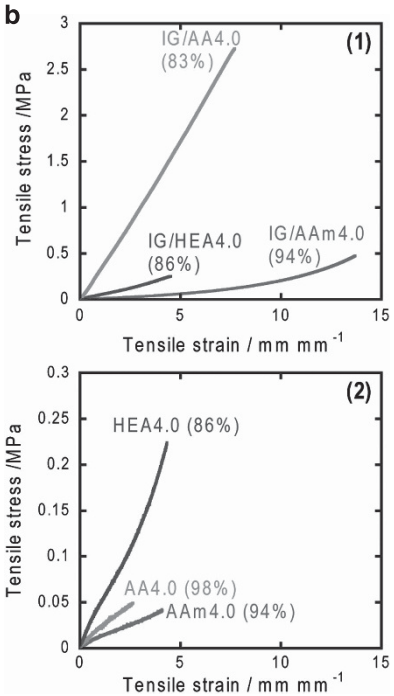

Figure 5 (**a**) The phase states of the mixtures of IG (5.0 w/v%) and polymers. (**b**) Typical tensile stress–strain curves of *in situ* polymerized (1) IG gels and (2) their reference gels. AA*X*, AAm*X* and HEA*X*, respectively, indicate the gels consisting of AA, AAm or HEA with *X* mol l^{-1} and 0.1 mol% of TEGDA versus vinyl monomer. The inserted percentage is the degree of swelling. A full color version of this figure is available at the *Polymer Journal* online.

swelling, with 93–94, 86 and 83% water content for the IG-AAm, IG-HEA and IG-AA gels, respectively.

The IG-AA gel exhibits extremely high breakdown stress compared with that shown by the IG-AAm gel. Strong anchoring is possible when every aluminol group on the outer wall of IG interacts with an AA molecule; a theoretical limit of 0.83 mol l^{-1} of the existing 4.0 mol l^{-1} would enable such anchoring. *In situ* polymerization produces 'polymerized sheaths', from which PAA strands grow outward by consuming the remaining 3.17 mol l^{-1} portion. Crosslinking among the sheaths occurs by radical recombination of the propagating PAA strands.

Polymer sheaths also form in the IG-HEA gel. However, the breakdown stress and strain of the IG-HEA gel are much lower than those of the IG-AA gel. Because the mechanical strength of an ordinary AA gel is lower than that of an ordinary HEA gel in the absence of IG nanotubes, the physical properties of IG gels are strongly dependent on the molecular structure of organic polymers. Both the IG-AA and IG-HEA systems exhibit strong variations in mechanical strength owing to the multiple interaction points between IG and organic polymer in the IG-AA and IG-HEA gels compared with those in the IG-AAm gel. Here the C=O and COOH groups of PAA interact with Al-OH[29] on IG in the IG-AA gel; in contrast, only the OH groups of PHEA interact with Al-OH on IG. It seems that the number of interacting groups between IG and organic polymer determines the mechanical properties of IG/organic polymer gels.

Thus the physical properties of IG gels drastically change with the manner of interaction between IG and organic polymer (that is, tying or sheathing). Essentially, the tying of the polymer to the IG nanotubes (IG-AAm system) produces stretchable IG gels; in contrast, the sheathing of the polymer on the IG nanotubes (IG-AA and IG-HEA systems) results in stiff IG gels, depending on the strength of interaction between the IG and the organic polymer.

STRAIN-INDUCED REVERSIBLE ISOTROPIC–ANISOTROPIC STRUCTURAL TRANSITION OF ROBUST IG HYDROGELS

The hydrogels consisting of IG and organic polymers exhibit birefringence only upon stretching, in the same manner as the shear-oriented IG-MA gels shown in Figure 3b. Such ordering of IG (Figure 6a) is reversible upon stretching and releasing cycles at a tensile strain that is smaller than the gel breakdown point. The birefringence Δn value of the IG-AAm gel (2.0 mol l^{-1} of [AAm]) is plotted as a function of the strain (Figure 6b). The Δn of the IG-AAm gel increases with tensile strain until 3.0 mm mm^{-1}, that is, Δn reaches $>5.3\times10^{-5}$ at strain = 3.0 mm mm^{-1}. The IG-AAm gel is optically isotropic when unstretched (at strain = 0) but exhibits positive birefringence under strains between 0.5 and approximately 8.5 mm mm^{-1} owing to the elongation-induced IG orientation. However, the birefringence decreases to negative values after further elongation (see the optical retardation photographs inserted in Figure 6b). As elucidated from the POM and optical retardation images,[21] IGs in pure water shows an optically positive birefringence, whereas PAAm is known to produce a negative birefringence after the elongation-induced molecular orientation.[30–33] Indeed, the ordinary crosslinked PAAm gel without IG exhibits a steady decrease of birefringence from zero to a negative value with increasing strain increments, as shown by the black plots in Figure 6b. Therefore, the bell-shaped profile of the Δn–strain curve of the IG-AAm gel in Figure 6b is the sum of both positive and negative birefringence effects[34] derived from the ordering of IG filaments and PAAm strands upon stretching. Other robust IG hydrogels (IG-AA/HEA gels) also show the reversible Δn change in response to strain.[26]

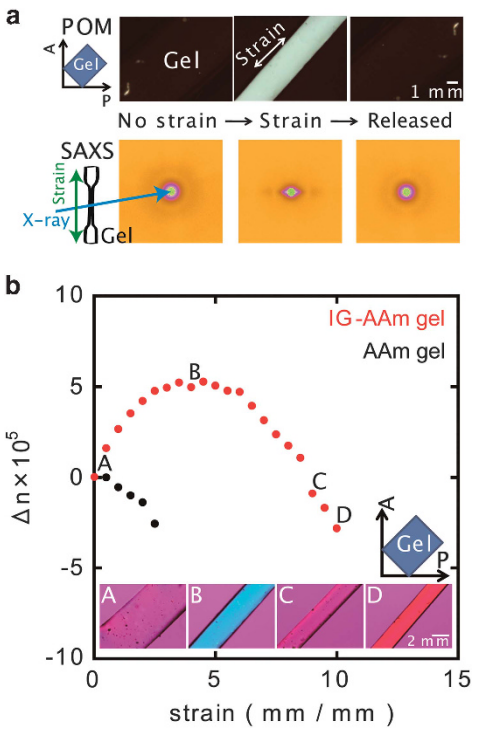

Figure 6 (**a**) POM images and two-dimensional SAXS patterns of an IG-AAm gel with ('Strain') or without ('No strain and Released') stretching at strain = 3.0. (**b**) Strain-induced Δn change of IG-AAm gels without (red plot) crosslinker and of an ordinary AAm gel (black plot). The measurements were carried out until gel fracture. The inserted images are the optical retardation (L = 530 nm) of IG-AAm gels at strain = 0 (A), 4.0 (B), 9.0 (C) and 10.0 (D).

ELECTRO-STIMULUS-RESPONSIVE BEHAVIOR OF IG DISPERSIONS

Finally, the specific electro-stimulus-responsive behavior of IG dispersions that encouraged to design IG-based supramolecular architectures for various electro-responsive materials is described. Recently, an aqueous suspension of hectorite particles in the deionized state that showed a change in viscosity upon the application of a direct-current (DC) electric field of the order of a few V mm^{-1} has been reported.[35] It is possible that the electrical double layer (EDL) may be easily deformed by applying an electric field and that this deformation would weaken the repulsive forces among the particles and result in the formation of a three-dimensional network structure. The good dispersibility of IG in aqueous media and its (de)protonation equilibria also encouraged to estimate the electro-stimuli-response of IG aqueous suspensions, as shown in hectorite aqueous suspension.[36] Here a reversible viscosity change of an IG aqueous suspension responding to an electric field was first observed (that is, the electrorheological (ER) effect). Then, using TEM, a structural assessment of the suspended IGs after the application of an electric field was performed.

The ER effect consists of reversible rheological property changes upon the application and removal of an electric field from materials.[37,38] Because of the reversible response to the electric field, the ER effect has been of interest not only in academic investigations but also in industrial applications.[39] Previously, it has been reported that suspensions of particles with various shapes (for example, nano-fibrous polyaniline[40] and titanium-silicon-coated carbon nanotubes[36]) show an ER effect under an electric field of several kV mm^{-1}.

The electro-stimuli-response of a 0.27 wt% (ϕ = 0.001) IG suspension with a low viscosity was estimated (that is, it behaves as a typical Newtonian fluid). By applying an electric field to the suspension, the shear stress σ increases, and the IG suspension behavior becomes non-Newtonian under a DC electric field >6.0 V mm^{-1} (Figure 7a). Below a DC electric field of 8.0 V mm^{-1} and a 19-s^{-1} shear speed, the σ gradually increases and reaches 0.14 Pa (Figure 7b). Then the removal of the DC electric field and continuous shear causes the decline of σ. The fact that the shear stress is recoverable by removing the electric field suggests that this system, under the electric field, exists in a secondary minimum of the potential energy curve, in light of classical DLVO theory.

After the application of the electric field, the IG suspension exhibits a gold color, that is, the transmittance of the suspension at 450 nm (T_{450}) changes from 100% to 82%. In the TEM images of suspension dried after the application of the electric field, the IGs assemble into thick bundles (Figure 8a (2)). Continuous shear after the removal of the electric field diminishes the gold color of the suspension (T_{450} = 90%) that corresponds to the disassembly of the thick IG bundles, as shown by the TEM image (Figure 8a (3)).

These results indicate that IG assembly/disassembly causes reversible increases/decreases in the σ value, producing the ER effect in the IG suspension. Reducing/recovering in the EDL of the IG surface by applying/removing an electric field brings about the assembly/disassembly of the IG nanotubes (Figure 8b). This type of IG assembly

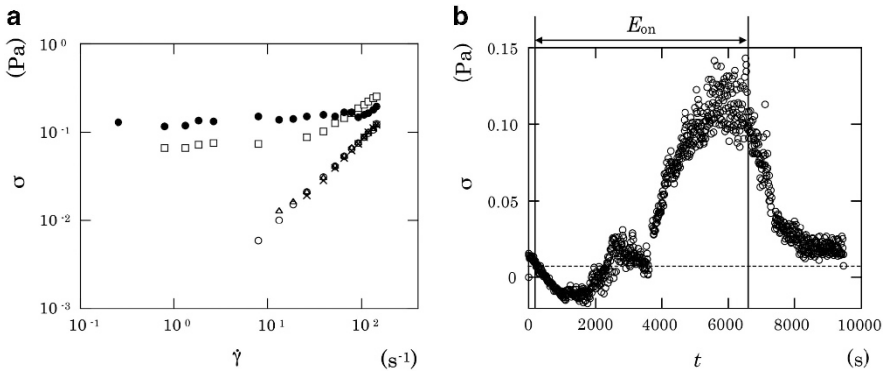

Figure 7 (**a**) The shear stress σ dependency as a function of shear rate $\dot{\gamma}$ for IG suspensions under different DC electric fields: open circles, 0 V mm^{-1}; crosses, 2.0 V mm^{-1}; triangles, 4.0 V mm^{-1}; squares, 6.0 V mm^{-1}; and closed circles, 8.0 V mm^{-1}. (**b**) The change in the shear stress σ for an IG suspension without a DC electric field (t=0–200 and 6500–9500 s) or with the application of an 8.0-V mm^{-1} DC electric field (t=200–6500 s) under 19 s^{-1} of shear rate. The broken line indicates the value of the water.

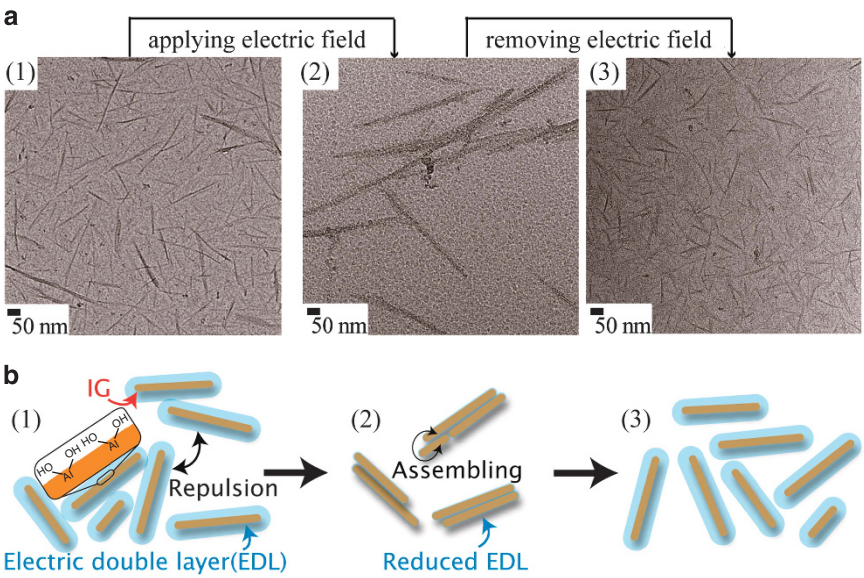

Figure 8 (**a**) TEM images of IGs in suspension (1) before (t=0 s in Figure 6b), (2) after applying an 8-V mm^{-1} DC electric field (t=6500 s in Figure 7b) or (3) after aging without a DC electric field via applying an 8-V mm^{-1} DC electric field (t>9500 s in Figure 7b). (**b**) Schematic illustration of the reversible IG assembly/disassembly owing to the reducing/recovering of their EDL in response to the application/removal of the electric field. (1)–(3) correspond to the (1)–(3) of panel (**a**).

also occurs under high pH conditions owing to the decreasing electric field intensity of the IG surface.[41] The ER effect of IG suspensions is unique because it emerges in an aqueous system under an electric field of a few V mm^{-1}; typical nanotubular suspensions need an electric field of several kV mm^{-1} for emergence of the ER effect.[39,40]

CONCLUSION

In this focused review, stimuli-responsive materials consisting of the rigid cylindrical inorganic polymer IG is described. The obtained materials exhibit thixotropy in response to mechanical shock,[22] physical anisotropy owing to oriented structures,[27,42] reversible isotropic–anisotropic structural transitions in response to strain[21,26,43,44] and an ER effect.[45] Here the careful design of interaction between IG and other organic molecules produced the materials with responsiveness to various stimuli. The manner of supramolecular assembly demonstrated in this study might apply to the design method of other hybrid materials consisting of rod-like polymers.[46–53] The presented experimental system yields structure-derived functional materials based on nanofiber assemblies that may contribute to various industrial/biomaterial applications of supramolecular architectures, such as mechano-chemical sensors, artificial biological tissues and high-efficiency ER actuators and valves.

CONFLICT OF INTEREST

The author declares no conflict of interest.

ACKNOWLEDGEMENTS

I thank Professor Emeritus Kiyotaka Shigehara of Tokyo University of Agriculture and Technology and Professor Emeritus Yoshihito Osada of Hokkaido University (RIKEN) for their guidance and to all my collaborators for developing the studies. This work was financially supported by grants from JSPS KAKENHI Grant Numbers 26870179 and 2555055 and the JGC-S Scholarship Foundation (No. 1335). The synchrotron radiation experiments were performed at BL40B2 and BL45XU in SPring-8 with the approval of the Japan Synchrotron Radiation Research Institute (JASRI) (Proposal Nos. 2011A1116, 2011B1407 and 2012B1140).

1 Howard, J. *Mechanics of Motor Proteins and the Cytoskeleton* (Sinauer Assoc. Inc., Sunderland, MA, USA, 2001).
2 Yu, Y., Nakano, M. & Ikeda, T. Photomechanics: directed bending of a polymer film by light. *Nature* **425**, 145 (2003).
3 Osada, Y. & Matsuda, A. Shape memory in hydrogels. *Nature* **376**, 219 (1995).
4 Liu, F. & Urban, M. W. Recent advances and challenges in designing stimuli-responsive polymers. *Prog. Polym. Sci.* **35**, 3–23 (2010).
5 Watanabe, J. & Takashina, Y. Columnar liquid crystals in polypeptides. 1. A columnar hexagonal liquid crystal observed in poly(γ-octadecyl L-glutamate). *Macromolecules* **24**, 3423–3426 (1991).
6 Okoshi, K., Kamee, H., Suzaki, G., Tokita, M., Fujiki, M. & Watanabe, J. Well-defined phase sequence including cholesteric, smectic a, and columnar phases observed in a thermotropic LC system of simple rigid-rod helical polysilane. *Macromolecules* **35**, 4556–4559 (2002).
7 Tokita, M., Shikinaka, K., Hoshino, T., Fujii, K., Mikami, J., Koshimizu, N., Sakajiri, K., Kang, S., Watanabe, J. & Shigehara, K. Thermotropic behavior of syndiotactic polymethylenes with alkyloxycarbonyl side chains. *Polymer* **54**, 995–998 (2013).
8 Koshimizu, N., Aizawa, Y., Sakajiri, K., Shikinaka, K., Shigehara, K., Kang, S. & Tokita, M. Thermotropic behavior of syndiotactic polymethylenes with ω-[4-(trans-4-Pentylcyclohexyl) phenoxy]alkyloxycarbonyl side chains. *Macromolecules* **48**, 3653–3661 (2015).
9 Cradwick, P. D. G., Farmer, V. C., Russell, J. D., Masson, C. R., Wada, K. & Yoshinaga, N. Imogolite, a hydrated aluminium silicate of tubular structure. *Nature Phys. Sci.* **240**, 187–189 (1972).
10 Bursill, L. A., Peng, J. L. & Bourgeois, L. N. Imogolite: an aluminosilicate nanotube material. *Philos. Mag. A* **80**, 105–117 (2000).
11 Mukherjee, S., Bartlow, V. M. & Nair, S. Phenomenology of the growth of single-walled aluminosilicate and aluminogermanate nanotubes of precise dimensions. *Chem. Mater.* **17**, 4900–4909 (2005).
12 Levard, C., Masion, A., Rose, J., Doelsch, E., Borschneck, D., Dominici, C., Ziarelli, F. & Bottero, J.-Y. Synthesis of imogolite fibers from decimolar concentration at low temperature and ambient pressure: a promising route for inexpensive nanotubes. *J. Am. Chem. Soc.* **131**, 17080–17801 (2009).
13 Farmer, V. C., Adams, M. J., Fraser, A. R. & Palmieri, F. Synthetic imogolite: properties, synthesis, and possible applications. *Clay Miner.* **18**, 459–472 (1983).
14 Farmer, V. C., Fraser, A. R. & Tait, J. M. Synthesis of imogolite: a tubular aluminium silicate polymer. *J. Chem. Soc. Chem. Commun.* **13**, 462–463 (1977).
15 Donkai, N., Inagaki, H., Kajiwara, K., Urakawa, H. & Schmidt, M. Dilute solution properties of imogolite. *Makromol. Chem.* **186**, 2623–2638 (1985).
16 Yamamoto, K., Otsuka, H., Wada, S., Sohn, D. & Takahara, A. Transparent polymer nanohybrid prepared by in situ synthesis of aluminosilicate nanofibers in poly(vinyl alcohol) solution. *Soft Matter* **1**, 372–377 (2005).
17 Larson, R. G. *The Structure and Rheology of Complex Fluids* (Oxford University Press, Oxford, UK, 1999).
18 Barnes, H. A. Thixotropy—a review. *J. Non-Newtonian Fluid Mech.* **70**, 1–33 (1997).
19 Cheng, X., McCoy, J. H., Israelachvili, J. N. & Cohen, I. Imaging the microscopic structure of shear thinning and thickening colloidal suspensions. *Science* **333**, 1276–1279 (2011).
20 Xu, X., Rice, S. A. & Dinner, A. R. Relation between ordering and shear thinning in colloidal suspensions. *Proc. Natl Acad. Sci. USA* **110**, 3771–3776 (2013).
21 Shikinaka, K., Koizumi, Y., Kaneda, K., Osada, Y., Masunaga, H. & Shigehara, K. Strain-induced reversible isotropic- anisotropic structural transition of imogolite hydrogels. *Polymer* **54**, 2489–2492 (2013).
22 Shikinaka, K., Kaneda, K., Mori, S., Maki, T., Masunaga, H., Osada, Y. & Shigehara, K. Direct evidence for structural transition promoting shear thinning in cylindrical colloid assemblies. *Small* **10**, 1813–1820 (2014).
23 Porod, G. in *Small-Angle X-Ray Scattering* (eds Glatter, O. & Kratky, O.) (Academic Press, London, UK, 1982).
24 Schmidt, P. W. *The Fractal Approach to Heterogeneous Chemistry* (John Wiley & Sons, New York, USA, 1989).
25 Ruzicka, B., Zaccarelli, E., Zulian, L., Angelini, R., Sztucki, M., Moussaïd, A., Narayanan, T. & Sciortino, F. Observation of empty liquids and equilibrium gels in a colloidal clay. *Nat. Mater.* **10**, 56–60 (2011).
26 Shikinaka, K., Yokoi, T., Koizumi-Fujii, Y., Shimotsuya, M. & Shigehara, K. Robust imogolite hydrogels with tunable physical properties. *RSC Adv.* **5**, 46493–46500 (2015).
27 Kaneda, K., Uematsu, K., Masunaga, H., Tominaga, Y., Shigehara, K. & Shikinaka, K. Flow-orientation of internal structure and anisotropic properties on hydrogels consisted of imogolite hollow nanofibers. *Sen'I Gakkaishi* **70**, 137–144 (2014).
28 Harsh, J. B., Traina, S. J., Boyle, J. & Yang, Y. Adsorption of cations on imogolite and their effect on surface charge characteristics. *Clays Clay Miner.* **40**, 700–706 (1992).
29 Yang, H., Chen, Y. & Su, Z. Microtubes via assembly of imogolite with polyelectrolyte. *Chem. Mater.* **19**, 3087–3089 (2007).
30 Demus, D., Goodby, J., Gray, G. W., Spiess, H. W. & Vill, V. *Handbook of Liquid Crystals* (Wiley-VCH, Weinheim, 1998).
31 Farinato, R. S. Elongational flow-induced birefringence of polyacrylamide and poly (acrylamide-co-sodium acrylate). *Polymer* **29**, 2182–2190 (1988).
32 Gindl, W., Martinschitz, K. J., Boesecke, P. & Keckes, J. Changes in the molecular orientation and tensile properties of uniaxially drawn cellulose films. *Biomacromolecules* **7**, 3146–3150 (2006).
33 Ohno, T. & Nishio, Y. Molecular orientation and optical anisotropy in drawn films of miscible blends composed of cellulose acetate and poly(N-vinylpyrrolidone-co-methyl methacrylate). *Macromolecules* **40**, 3468–3476 (2007).
34 Murata, K. & Haraguchi, K. Optical anisotropy in polymer-clay nanocomposite hydrogel and its change on uniaxial deformation. *J. Mater. Chem.* **17**, 3385–3388 (2007).
35 Kimura, H., Sugiyama, T., Takahashi, S. & Tsuchida, A. Viscosity change in aqueous hectorite suspension activated by DC electric field. *Rheol. Acta* **52**, 139–144 (2013).
36 Oh, S. Y. & Kang, T. J. Electrorheological response of inorganic-coated multi-wall carbon nanotubes with core-shell nanostructure. *Soft Matter* **10**, 3726–3737 (2014).
37 Halsey, T. C. Electrorheological fluids. *Science* **258**, 761–766 (1992).
38 Hao, T. Electrorheological fluids. *Adv. Mater.* **13**, 1847–1857 (2001).
39 Block, H. & Kelly, J. P. Electro-rheology. *J. Phys. D Appl. Phys.* **21**, 1661–1677 (1988).
40 Yin, J., Zhao, X., Xia, X., Xiang, L. & Qiao, Y. Electrorheological fluids based on nano-fibrous polyaniline. *Polymer* **49**, 4413–4419 (2008).
41 Ma, Y. L. & Karube, J. Imogolite flocculation under alkaline conditions. *Soil Sci. Plant Nutr.* **59**, 125–129 (2013).
42 Shikinaka, K., Kikuchi, H., Maki, T., Shigehara, K., Masunaga, H. & Sato, H. Chiral-linkage-induced hierarchical ordering of colloidal achiral nanotubes in their thixotropic gel. *Langmuir* (in revision).
43 Shikinaka, K., Koizumi, Y. & Shigehara, K. Mechanical/optical behaviors of imogolite hydrogels depending on their compositions and oriented structures. *J. Appl. Polym. Sci.* **132**, 41691 (2015).
44 Shikinaka, K. & Shigehara, K. Ordered structurization of imogolite clay nanotubes by the spatiotemporal regulation of their assemblies. *Colloids Surf. A* **482**, 87–91 (2015).
45 Shikinaka, K. & Kimura, H. Reversible viscosity change of nanotubular polyelectrolyte aqueous suspensions. *Colloids Surf. A* **459**, 1–3 (2014).
46 Biette, L., Carn, F., Maugey, M., Achard, M.-F., Maquet, J., Steunou, N., Livage, J., Serier, H. & Backov, R. Macroscopic fibers of oriented vanadium oxide ribbons and their application as highly sensitive alcohol microsensors. *Adv. Mater.* **17**, 2970–2974 (2005).
47 Kaneko, Y., Sato, S., Kadokawa, J. & Iyi, N. Synthesis of organic-inorganic hybrid hydrogels using rodlike polysiloxane having acrylamido groups as a new cross-linking agent. *J. Mater. Chem.* **16**, 1746–1750 (2006).
48 Yang, W., Furukawa, H., Shigekura, Y., Shikinaka, K., Osada, Y. & Gong, J. P. Self-assembling structure in solution of a semirigid polyelectrolyte. *Macromolecules* **41**, 1791–1799 (2008).
49 Shikinaka, K., Kakugo, A., Osada, Y. & Gong, J. P. Mechanism of polarity sorting of actin bundles formed with polycations. *Langmuir* **25**, 1554–1557 (2009).
50 Kumar, K. D., Tsou, A. H. & Bhowmick, A. K. Unique tackification behavor of needle-like sepiolite nanoclay in brominated isobutylene-co-p-methylstyrene (BIMS) rubber. *Macromolecules* **43**, 4184–4193 (2010).
51 Shigehara, K., Kudoh, H., Sakai, T., Osada, Y., Murakami, Y. & Shikinaka, K. Thermoresponsive synthetic polymer-microtubule hybrids. *Langmuir* **29**, 11786–11792 (2013).
52 Jing, H., Higaki, Y., Ma, W., Xi, J., Jinnai, H., Otsuka, H. & Takahara, A. Preparation and characterization of polycarbonate nanocomposites based on surface-modified halloysite nanotubes. *Polym. J.* **46**, 307–312 (2014).
53 Shikinaka, K., Misu, M., Furukawa, H., Kakugo, A. & Gong, J. P. Anisotropic gelation induced by very little amount of filamentous actin. *Macromol. Chem. Phys.* **216**, 2007–2011 (2015).

Supplementary Information accompanies the paper on Polymer Journal website (http://www.nature.com/pj)

Dr Kazuhiro Shikinaka was born in Mie Prefecture, Japan in 1981. He received his Doctor of Philosophy in 2008 from Hokkaido University. Now he is an Assistant professor of Graduate School of Engineering, Tokyo University of Agriculture and Technology. Currently Dr Kazuhiro Shikinaka's researches focus on the creation of stimuli-responsive materials consisting of rigid inorganic cylindrical polymers, on the full utilization of plant biomass as basic chemical products and on the macroscopic self-organization of microtubules, which reflects their nanometer-size chiral structure. He was the recipient of Award for Encouragement of Research in Polymer Science; The Society of Polymer Science, Japan (2014), Award for Encouragement of Research in Fiber Science; The Society of Fiber Science and Technology Japan (2014), The CSSJ Best Presentation Award (Oral session); The Clay Science Society of Japan (2014) and FAPS YOUNG SCIENTIST POSTER AWARD in 2009.